Published in final edited form as:
J Neurosci Methods. 2010 May 30; 189(1): 5–13. doi:10.1016/j.jneumeth.2010.02.017.

A microfluidic brain slice perfusion chamber for multisite recording using penetrating electrodes

Alexander J. Blake[1], **Frank C. Rodgers**[2], **Anna Bassuener**[2], **Joseph A. Hippensteel**[1], **Thomas M. Pearce**[1,3], **Timothy R. Pearce**[1], **Ewa D. Zarnowska**[2], **Robert A. Pearce**[2], and **Justin C. Williams**[1]

[1]Department of Biomedical Engineering, University of Wisconsin, Madison, WI 53705

[2]Department of Anesthesiology, University of Wisconsin, Madison, WI 53711

Abstract

To analyze the spatiotemporal dynamics of network activity in a brain tissue slice, it is useful to record simultaneously from multiple locations. When obtained from laminar structures such as the hippocampus or neocortex, multisite recordings also yield information about subcellular current distributions via current source density analysis. Multisite probes developed for *in vivo* recordings could serve these purposes *in vitro*, allowing recordings to be obtained from brain slices at sites deeper within the tissue than currently available surface recording methods permit. However, existing recording chambers do not allow for the insertion of lamina-spanning probes that enter through the edges of brain slices. Here, we present a novel brain slice recording chamber design that accomplishes this goal. The device provides a stable microfluidic perfusion environment in which tissue health is optimized by superfusing both surfaces of the slice. Multichannel electrodes can be inserted parallel to the surface of the slice, at any depth relative to the surface. Access is also provided from above for the insertion of additional recording or stimulating electrodes. We illustrate the utility of this recording configuration by measuring current sources and sinks during theta burst stimuli that lead to the induction of long-term potentiation in hippocampal slices.

Keywords

microfluidics; hippocampus; field potentials; action potential; long-term potentiation (LTP); current source density (CSD); multisite recording electrodes

Introduction

The brain is composed of ensembles of small- and large-scale neuronal networks that, spontaneously or upon stimulation, generate coordinated activity patterns. In order to acquire information about the underlying spatiotemporal dynamics it is useful to record activity simultaneously at multiple locations (Csicsvari et al., 2003B). In laminated neural

Corresponding author: Dr. Justin C. Williams Assistant Professor University of Wisconsin Department of Biomedical Engineering #2150 Engineering Centers Building 1550 Engineering Drive Madison, WI 53706, USA jwilliams@engr.wisc.edu office 608 265 3952 fax 608 265 9239.

[3]Current address: Department of Anatomy and Neurobiology, Washington University in St Louis School of Medicine, St. Louis, MO 63130

structures, additional information can be obtained by using current source density (CSD) analysis to derive the distribution of synchronous membrane events that give rise to the measured voltage fluctuations (Freeman and Nicholson, 1975; Mitzdorf, 1985; Buzsáki et al., 1986; Taube and Schwartzkroin, 1988; Vida et al., 1995). Penetrating multisite linear recording arrays have been developed that can be used for these purposes *in vivo*. The electrode sites are configured for specific electrophysiological applications by roughly matching them with the tissue cytoarchitecture (Buzsáki et al., 2004).

Brain slice preparations offer an alternative recording environment. For investigations of network patterns of activity, they provide a number of advantages over *in vivo* preparations, including the ability to record from discrete brain regions that maintain cytoarchitecturally preserved units of neuronal networks removed from the influence of afferent pathways (Sarvey et al., 1989; Traub et al., 1989). More importantly, *in vitro* brain slice recording methods offer a substantially greater control over certain experimental parameters (e.g. temperature, pH, pharmacological modulation), greatly facilitating investigations into the cellular mechanisms that underlie network activity.

A number of *in vitro* recording devices have been developed that incorporate multiple recording sites, including planar and three-dimensional microelectrode arrays (MEAs), which are capable of recording and stimulating at the sub-millimeter scale (Boppart et al., 1992; Csicsvari et al., 2003A; Gholmieh et al., 2006; Berdichevsky et al., 2009). Unfortunately, signals that originate from intact networks within the interior of slices are degraded at the injured tissue surfaces (Aitken et al., 1995), and this adversely affects the signal-to-noise ratio in recordings obtained from planar MEA recordings. This problem can be partially overcome using three-dimensional MEAs that penetrate the injured surface (Heuschkel et al., 2002; Nam et al., 2006), but this approach itself suffers from a combination of a limited recording depth and the need to obtain recordings near the non-perfused surface of the brain slice. Penetrating multisite linear electrodes potentially offer the ability to record from deep within tissue where neural networks are intact and active, while maintaining some of the same recording advantages as MEAs (Buzsáki, 2004). However, existing *in vitro* recording chambers lack access features that permit the realization of this recording configuration (Passeraub et al., 2003; Mohammed et al., 2008).

We sought to design an *in vitro* brain slice perfusion chamber that would enable extracellular recordings of network activity using a penetrating multisite electrode inserted parallel to the surface of the tissue slice, at any tissue depth, and that would incorporate laminar solution flow across both surfaces of the slice to enhance tissue viability (Passeraub et al., 2003; Rambani et al., 2009; Hájos et al., 2009). The perfusion chamber that we designed, built, and tested utilizes arrays of microposts that immobilize the tissue slice while providing fluid flow to both surfaces for delivery of oxygen and nutrients. In addition, it incorporates a lateral opening that permits the insertion of a penetrating multisite linear-array recording electrode into the edge of the slice, and an opening in the top for insertion of stimulating or conventional recording electrodes. We illustrate the utility of this recording configuration by measuring evoked activity in the CA1 area of a hippocampal brain slice undergoing long-term potentiation of excitatory synaptic strength by theta-burst stimulation, and apply current source density analysis to reveal patterns of current flow during the potentiating stimulus.

Materials and methods

Chamber Design

The microfluidic perfusion device used in this study is fabricated from poly-dimethyl-siloxane (PDMS, Sylgard 184, Dow Corning, Midland, MI). The process involves pouring a

liquid pre-polymer onto a microfabricated mold, curing the polymer, and then releasing the resulting solidified material from the mold (Duffy et al., 1998). The final step requires that structural features of the mold do not mechanically impede the removal of the cured PDMS. Given this limitation, forming an enclosed 3-dimensional structure such as a microfluidic channel requires bonding the cured PDMS to another surface (Jo et al., 2000).

Perfusing both surfaces of a brain slice preparation enhances tissue viability for *in vitro* electrophysiology experiments (Rambani et al., 2009; Hájos et al., 2009). To accomplish this, we use a multi-stage process in which three layers of PDMS are individually molded, then bonded together via an oxygen-plasma surface treatment (Fig. 1). The first layer consists of a micropost array within a microfluidic channel. The brain slice is supported by the micropost array while the bottom surface of the tissue is perfused via the fluid channel. The second PDMS layer encloses the lower channel except for an opening located above the micropost array, which houses the slice. The shape of this opening closely fits the size and shape of the slice, and the thickness of the PDMS is matched to that of the tissue. The third layer of the chamber closely resembles the first, with a micropost array to hold the slice in place and a microfluidic channel to perfuse the upper surface.

An important, and novel, feature of our chamber is the inclusion of electrode access ports into the otherwise enclosed microfluidic environment surrounding the brain slice. Each port is an opening in the channel wall that connects the interior of the device with the exterior. The hydrophobic properties of the PDMS, combined with the small dimensions of the electrode access ports, create surface-tension “virtual walls” at these openings. Through these virtual-wall access ports, electrodes can be inserted into the slice and the perfusion bath without causing fluid to spill out of the microfluidic channels, maintaining laminar flow over both surfaces of the slice. It is important to note that this principle is not limited to the top surface of the chamber – in our device, an opening in the lateral wall of the second PDMS layer allows a multisite linear-array recording electrode to horizontally penetrate the edge of the slice, parallel to the surface. This reproduces the electrode placement used in *in vivo* experiments (Buzsáki, 2004; Ward et al., 2009), and would be difficult to accomplish using conventional perfusion chambers.

Fabrication Procedure

The process for forming each PDMS layer is based on standard photolithography and microfabrication techniques utilizing silicon master molds (Jo et al., 2000). For this device, we use a monomer:crosslinker ratio of 10:1. The monomer and crosslinker are mixed by hand until the mixture becomes opaque with bubbles, and then degassed in a vacuum chamber to remove bubbles before being pouring onto the mold. The PDMS is cured at 95°C for 2 hours and slowly cooled to 40°C before removing the solidified polymer from the mold.

Master molds for each layer are photo-patterned with ultraviolet light. First, a silicon wafer is spin-coated with a photoresist (SU8 2100, MicroChem Corp., Newton, MA) according to the manufacturer’s specifications, and heated to 65°C for 7 minutes and 95°C for 1 hour in a pre-exposure baking step. Next, the wafer with photoresist is exposed to ultraviolet light (λ= 365nm) through a printed mask containing the design for the layer. Typically, a silicon master is a negative of the desired structure, and the final PDMS features are molded directly from this master. The middle PDMS layer is formed from this type of conventional negative master mold. In contrast, the top and bottom layers make use of a double casting process that serves to increase the fabrication yield of the high-aspect-ratio micropost arrays (Blake et al., 2007; Sniadecki and Chen, 2007). The features of the bottom and middle layers are of a uniform thickness, so a single coating of photoresist is sufficient. For the top layer, a second photoresist spin and UV exposure is used to create the electrode access ports on the

top surface of the device (Fig. 2D). Following UV exposure, the wafers are post-exposure baked at 65°C for 5 minutes and 95°C for 20 minutes. Finally, the unexposed photoresist is removed with a developer solvent to form the master mold. A schematic of the procedure is shown in Fig. 2.

Next, PDMS is poured onto the silicon master molds and cured. Since the silicon wafers for the top and bottom layers were exposed to *positive* images of the desired structure, curing polymer on these masters yields a flexible *negative* PDMS master mold (Fig. 2D). A silane gas treatment of the PDMS master prevented uncured PDMS from adhering to the surface (Sniadecki and Chen, 2007). Afterwards, these masters can be used to form the final top and bottom PDMS layers (Fig. 2B). For these layers, the channel depth and micropost height are 250 μm, which is defined by the thickness of the photoresist layer on the original silicon master. The double casting process, which utilizes a flexible PDMS master, is useful because the microposts (250 μm diameter) are difficult to release from a conventional rigid silicon master mold (Sniadecki and Chen, 2007). The middle layer, which houses the brain slice, requires a thickness matched to that of the tissue (in our case 500 μm) (Wu et al., 2004), which is also defined by the depth of the photoresist spin-coated onto the silicon wafer. To create a PDMS layer of uniform depth with a fully-penetrating space for the slice, we forced excess pre-polymer out of the master by applying pressure onto the photoresist features from above (Fig. 2C). Finally, the three PDMS layers are aligned and bonded together via oxygen-plasma surface treatment (Jo et al., 2000), leaving the outflow end of the top layer unbonded so slices can be easily inserted into the chamber.

Hippocampal slice preparation

All procedures were conducted according to the guidelines laid out in the *Guide for the Care and Use of Laboratory Animals* and approved by the University of Wisconsin Animal Care and Use Committee, Madison, Wisconsin. Mice were housed in an animal care facility under 12-hr cycles of light and dark. They had continuous access to food and water.

Brain slices were made from 5-7 week old male offspring of 129×1/SvJ (RCC, Fullinsdorf, Switzerland) breeding pairs. Mice were anesthetized with 2.5% isoflurane and decapitated. Heads were immediately submerged in ice-cold “dissection solution” that contained (in mM): NaCl 127, KCl 1.9, K_2HPO_4 0.8, $NaHCO_3$ 26, $MgSO_4$ 2.7, $CaCl_2$ 0.9, glucose 15, ascorbic acid 1, kynurenic acid 1 (Sigma) and saturated with 95% O_2 / 5% CO_2. After opening the skull, the brain was extracted and blocked by cutting off the cerebellum and prefrontal cortex. The brain was glued to a microtome slice tray with cyanoacrylate glue and 500 μm-thick coronal slices were cut using a vibrating microtome (Leica VT 1000S, Leica Microsystems, Nussloch GmbH, Nusslock, Germany). A portion of the slice that included the hippocampus was trimmed with a scalpel to provide for proper fit within the recording chamber. Brain slices recovered in a holding chamber filled with carbogenated artificial cerebrospinal fluid (ACSF) that contained (in mM): NaCl 127, KCl 1.9, K_2HPO_4 0.8, $NaHCO_3$ 26, $MgSO_4$ 1.44, $CaCl_2$ 2.17, glucose 15, for at least 1h at room temperature (20-22°C). Then slices were transferred to the recording chamber using a wide-open Pasteur pipette. The chamber was perfused with ACSF at a flow rate of 2.5 ml/min, although laminar flow rates up to 6 ml/min have been shown to maintain network oscillations in hippocampal slices (Hájos et al., 2009). Experiments were performed at 30 ± 1°C. The recording solution temperature was controlled with an in-line temperature controller (Warner Instruments Corp., Hamden, CT). To prevent air/gas bubble formation, the solution reservoir containing ACSF was bubbled with carbogen at 38°C, and the temperature of the air surrounding the recording chamber was maintained at ~30°C using a forced-air patient warming system (Bair Hugger, Augustine Medical Inc., Eden Prairie, MN).

Electrode insertion and electrophysiological recordings

Extracellular potentials were recorded using a 16-channel linear-array recording electrode with iridium metal sites spaced 50 μm apart on a single shank 3 mm in length and 15 μm thick (NeuroNexus Technologies, Ann Arbor, MI) (Fig. 3). The linear-array recording electrode has a relatively small cross-sectional area (15×150 μm) and a sharp tip design that allowed it to effectively penetrate and cut through tissue with minimal damage (Bjornsson et al., 2006). Output pins from the linear-array recording electrode plugged directly into a 16-pin DIP socket custom interface that was mounted on a digital micromanipulator (Siskiyou Corporation, Grants Pass, OR) and attached to a buffer/preamp head stage (Neuralynx Inc., Tucson, AZ). Under visual control, the manipulator was used to maneuver the linear-array recording electrode into the brain slice, by inserting it through the "virtual wall" opening in the brain slice chamber and into the edge of the brain slice, 100-200 μm below its top surface. The electrode was advanced until the tip reached the hippocampal fissure. We did not take any measures to optimize the recording depth that we used; we selected 100-200 μm based on our previous experience using sharp electrodes for extracellular recordings (Pearce, 1993, 1996), and it is possible that larger signals would have been obtained had the depth been optimized. Using the stereomicroscope, we were able to consistently insert the electrode in tissue slices at a speed of ~100 μm/s without encountering any compression that could result in lifting, warping or tearing of the tissue slice (Bjornsson et al., 2006). Viability of cells adjacent to the recording electrode sites was confirmed by recording spontaneous single-unit activity (Drake et al., 1988; Vetter et al., 2004, our data not shown).

Platinum/iridium concentric bipolar stimulating electrodes (FHC, Bowdoin, ME) inserted into *stratum radiatum* (SR) were used to activate the Schaffer collateral excitatory afferent pathway in the CA1 region (Fig. 3). Stimuli were delivered using a constant current stimulus isolator (model A365D, World Precision Instruments, Sarasota FL). Signals were amplified, low pass filtered at 3 kHz (LYNX-8 amplifiers, Neuralynx, Inc, Tucson, AZ), digitized at 10 kHz using an analog-to-digital converter (Digidata 1440A, Molecular Devices, Sunnyvale, CA), and acquired using pClamp software (Version 10.2, Molecular Devices, Sunnyvale, CA).

Long-term potentiation (LTP) was evoked using a "triple theta burst stimulation" (TBSx3) protocol (Larson et al., 1986). TBSx3 consisted of three TBS trains at one-minute intervals. A single TBS train consisted of bursts of 5 stimuli delivered at 100 Hz, repeated 10 times at an interval of 200 ms, using a stimulus intensity (70-270 μA x 0.1 ms) that evoked a half-maximal population spike (PS). Test stimuli using lower stimulus intensities (38-70 μA x 0.1 ms) that evoked field excitatory postsynaptic potentials (fEPSPs) below PS threshold were applied at one-minute intervals (0.016 Hz). Baseline responses were considered stable if fEPSPs varied by less than 10% over the 10 minutes preceding TBS.

Electrophysiological data analysis

To assess LTP of the fEPSP, we used the channel in *stratum radiatum* (SR) that had the greatest slope prior to LTP induction. This channel was typically located 100-150 μm from the fEPSP "null point", which corresponds to the border between SR and *stratum pyramidale* (SP) (Richardson et al., 1987). Data were analyzed using Clampfit (Version 10.2, Molecular Devices, Sunnyvale, CA). The slope of each fEPSP was normalized to the average of the 10 responses just preceding TBS. Potentiation of the fEPSP was expressed as the fractional increase in the average of the normalized values between 50 to 60 min following TBSx3. PS amplitudes were measured from the channel at the "null point" for evoked fEPSPs, using AxoGraphX (Version 1.2.1, Molecular Devices, Sunnyvale, CA).

Current source density (CSD) analysis was used to derive the magnitudes of the current sources and sinks along the axis of the CA1 cells during TBSx3. We used an implementation of the CSD analysis based on the spline iCSD method developed by Pettersen and colleagues (Pettersen et al., 2006). We chose the spline method because it assumes a more realistic current distribution based on a columnar geometry of the underlying current source. Although there may be layer-specific differences in conductivity across laminated cortical structures, this has only a minor effect on the spatial profile of derived current sinks and sources (Holsheimer, 1987). Therefore, we assumed the conductivity to be uniform throughout the slice. CSD is expressed in units of $\mu A/mm^3$. We arbitrarily used warm colors (red and yellow) to represent current sinks and cold colors (blue) to represent current sources (Fig. 5).

Design considerations and troubleshooting

PDMS was chosen to construct the perfusion chamber because it offers many attractive physical and chemical properties in comparison to conventional perfusion chamber materials, such as short construction time, fabrication repeatability, optical transparency, low cost, and low toxicity (Beebe et al., 2002). In particular, PDMS allows the fabrication of prototype devices having microscale features within a matter of hours (Beebe et al., 2000). Rapid prototyping can be vital in minimizing the time to arrive at an optimal design configuration, after which devices can be batch-processed with relatively short turnover times. PDMS is optically transparent to wavelengths of 230-700 nm, thus enabling standard microscope objectives for viewing samples through PDMS layers. The material is well suited for making numerous perfusion devices since it is a fairly inexpensive, elastic polymer with a low permeability to water. PDMS is not toxic to cellular environments and can be easily integrated for a number of biological applications (Beebe et al., 2002; Berdichevsky et al., 2009). Hence, we developed a microfluidic perfusion device that uses inexpensive, easily modified materials providing maximum experimental flexibility. The material properties of this device meet the standards of existing perfusion chambers (*e.g.* sterility, optical compatibility, *etc.*), while offering additional flexibility to quickly change experimental parameters (*e.g.* adding more inputs, modifying center layer to fit different slice shapes or thicknesses, *etc.*).

Although PDMS does possess many useful characteristics, its porous nature can lead to the collection of potentially harmful gas bubbles in the enclosed chamber. In our initial tests we found that the appearance of gas bubbles along the walls of the fluid path was invariably detrimental to electrophysiological recordings, presumably because it led to poorly perfused areas of the slice. The formation of the gas bubbles depended on two factors: off-gassing from the PDMS, and out-gassing from the perfusate solution.

To address the off-gassing issue, we submerged the device in deionized water under vacuum for at least 2 hours before each experiment. After removing the device from the vacuum chamber, we dried the exterior portions of the device to ensure proper adhesion of the PDMS layers. In particular, it was critical to dry the area between the hinged area of the third PDMS layer and the second PDMS layer to prevent leaks from occurring. When dry, PDMS is notable for its ability to spontaneously adhere to itself. Keeping the hinged region dry allowed us to reposition the brain tissue slice between the microposts of the first and third layers, even repeatedly, to achieve an optimal orientation of the recording electrode along the axis of CA1 pyramidal cells.

Out-gassing of bubbles from the perfusate was addressed by controlling the perfusate and external temperature, a step that is necessary even with conventional recording chambers. To prevent the formation of microbubbles as the solution was re-warmed by an in-line heater just prior to its entry into the recording chamber, the temperature of the ACSF

reservoir was set at 38 °C. This greatly reduced bubble formation within the recording chamber. However, it did not completely prevent bubble formation during experiments lasting several hours. We found that warming the exterior air surrounding the chamber to within ~8 °C of the perfusate temperature was successful in preventing the formation of gas bubbles for experiments lasting up to 8 hours.

The perfusion recording chambers typically lasted for at least 20 experiments before failure. Chamber failure was due to physical damage of the PDMS from repeated folding of the top layer when inserting and removing brain slices. Additionally, with extended use, salt deposits decreased the hydrophobicity of the PDMS surface, and this could result in fluid leaking out of the chamber. However, when properly washed and maintained, the recording devices were functional for as long as a year with intermittent use, 40-50 experiments. After each experiment we carefully rinsed the chamber using ultrapure water to remove any salts remaining from the recording solution. Next we used isopropyl alcohol to remove tissue lipid residues and to dry the chamber. Chambers were stored in a dust free container to maintain surface characteristics. This maintenance protocol allowed us to reuse PDMS chambers until physical damage of the device occurred. The cleaning process was critical to maintaining a leak-free system.

Stimulating and recording electrodes were cleaned after each experiment by simply dipping in a beaker filled with ultrapure water and drying in air. Electrodes maintained in the fashion could be used daily for several months with little change in impedance.

Results

To demonstrate the ability of the brain slice chamber to maintain healthy tissue, we measured population responses in the hippocampal CA1 region following Schaffer collateral fiber stimulation. Electrical stimuli were applied to *stratum radiatum* (SR) using a bipolar stimulating electrode inserted perpendicular to the slice surface through an opening in layer 3 (Fig. 1B). Extracellular recordings of evoked activity were obtained using a 16-channel linear-array electrode inserted through an opening in layer 2. The electrode was inserted parallel to the surface of the slice, 100-200 μm below the upper surface, and with the tip positioned at the hippocampal fissure so that the recording sites spanned the layers of CA1 from the alveus to *stratum lacunosum-moleculare*.

Electrical stimuli induced population EPSPs in the dendritic layers, and action potentials that were evident as single “population spikes” (PS) at the *stratum pyramidale* (SP). In a total of 38 brain slices, the PS amplitude following supramaximal stimulation was 3.80 ± 1.39 mV (mean ± SD; range 2.10 - 7.10 mV). Responses were stable for up to 8 hours.

To illustrate the utility of this novel recording configuration, we induced LTP in a subset of slices, and used CSD analysis to derive spatiotemporal patterns of current sources and sinks during its induction. An example of the response induced by electrical stimulation subthreshold for an action potential generation prior to LTP induction is shown in Fig. 4A. It is apparent that the evoked fEPSP spanned several recording sites. We used the site with the greatest slope before LTP induction to assess synaptic strength (Fig. 4A, bold trace).

LTP induced by a triple theta burst stimulation (TBSx3) protocol (see Materials and Methods for stimulation details) resulted in an increase in the mean fEPSP slope of 30 ± 7% (mean ± SD) in this single experiment (Fig. 4B), and the appearance of a PS (most evident at the SP recording site). On average, TBSx3 led to an increase in fEPSP slope of 35 ± 10% ($p<0.05$, $n=4$) (Fig. 4C).

To assess the spatiotemporal pattern of evoked activity during the LTP-inducing TBS, we applied CSD analysis. Figure 5 illustrates the CSD profiles obtained during the 1st (Fig. 5A) and 21st (Fig. 5B) bursts in a 30-burst TBSx3 protocol. In response to the first stimulus, the afferent volley (*), which itself extends over several channels in the middle of SR, is followed by a forward-propagating PS (**) that initiates in the apical dendrite and propagates to the SP, and slightly into *stratum oriens* (SO). Subsequent stimuli in the burst lead to synaptic responses (# - sinks in SR aligned with the afferent volley) that are progressively longer-lasting with each stimulus, but these do not lead to action potentials in the pyramidal cells. The activity pattern elicited during the 21st burst is similar, except that the second stimulus in the burst now also produces a forward-propagating PS. Qualitatively similar results were obtained in each of the slices to which the TBSx3 protocol was applied.

Discussion

The goal of the presented study was to design, build, and test an *in vitro* microfluidic perfusion chamber for performing extracellular recordings, using linear-array multisite recording electrodes that were originally developed for use *in vivo*. This new *in vitro* configuration afforded us the advantages inherent to brain slice preparations, such as the ability to study isolated circuits in a controlled microenvironment, and at the same time allowed us to measure the spatial and temporal characteristics of neuronal network activity using high fidelity linear-array recording electrodes.

A number of different approaches have been taken previously to enable multisite recordings from acute and cultured brain slice preparations. MEAs that are constructed from various materials (e.g., metal, silicon), and organized in diverse geometries, have been reported in the literature (Rutten et al., 2001), and are even available commercially (Ayanda Biosystems, Lausanne, Switzerland). They allow users to record brain slice surface potentials from multiple sites simultaneously. However, signal amplitudes (10s to 100s of μV) are substantially smaller than those obtained using conventional glass electrodes (several mV), due to two factors: damage to surface cells during the slicing process, and recording from the non-perfused surface of the slice.

To record from sites deeper within the tissue, and thus nearer to the cells that generate the electrical signals, three-dimensional MEAs with protruding contacts have been developed (Heuschkel et al., 2002; Nam et al., 2006). This has led to an improved signal-to-noise ratio. But, even here, signals typically remain in the sub-millivolt range (Steidl et al., 2006). Presumably this reflects the limited height (60 μm) as well as geometry (conical protrusions that displace tissue) of the recording sites. To permit oxygen and nutrients to reach the tissue surface from which recordings are obtained, a perforated microelectrode array has also been developed (Boppart et al., 1992). Although the openings constituted only 6% of the recording surface, this did improve tissue longevity. Nevertheless, signals of only several hundred microvolts were obtained (Boppart et al., 1992). This may have been due in part to the use of surface electrodes, but it is likely that limited exchange through these openings also played a factor. Indeed, recent studies have highlighted the importance of maintaining high oxygen supply (Huchzermeyer et al., 2008), the need for high solution flow rates (Hájos et al., 2004), and the benefits of directing solution flow across both surfaces of brain slices (Hájos et al., 2009), for maintaining network activity *in vitro*. The amplitudes of the evoked responses that we recorded are similar to those typically obtained using conventional electrodes (Lipton et al., 1995), and substantially greater in amplitude than previously reported multisite recordings from brain slices. It is likely that both factors – recording from deep within the slice, and providing laminar flow of oxygenated ASCF to both slice surfaces to enhance viability (Blake et al., 2007) – played roles in bringing about this improvement. Another potential benefit of this approach is the small volume of the recording chamber and

the minimally exposed surface area through which oxygen can be lost. Recent studies have highlighted the importance of these two factors in maintaining healthy tissue slices with low solution flow rates (Hajos and Mody, 2009). In those experiments, a reduction in chamber volume from 2 mL to 0.5 mL permitted the solution flow rate to be reduced from 12-20 mL/min to 6 mL/min while still maintaining network activity requiring high levels of tissue oxygenation. Although we did not test the influence of changing solution flow rate in our experiments, the low chamber volume (0.062 mL) and the enclosed nature of the chamber design suggest that solution flow rates might be able to be reduced substantially from the 2.5 mL/min flow rate that we used here, while still maintaining adequate oxygenation.

By recording from multiple sites, the spatiotemporal pattern of current sinks and sources that give rise to the observed voltage deflections may be derived by CSD analysis (Wheeler and Novak, 1986). The spatial sampling rate should be at least twice that of the highest spatial frequency component in the distribution of extracellular current sinks and sources. For hippocampal slices, this is thought to require an electrode spacing of 100 μm (Bragin et al., 2000; Csicsvari et al., 2003A). The laminar profiles of field potentials that we obtained with 50 μm spaced electrodes were thus suitable for CSD analysis. The responses that we observed resembled in many respects those reported previously using extracellular single point electrodes moved between recording sites (Richardson et al., 1987), including an early sink in the dendrites associated with a passive source at the soma, and a superimposed strong sink at the soma that corresponds to the action potential (Fig. 5). However, the direction of population spike propagation in the apical dendrite differed in our studies; we found that the spike invariably moved from the dendrite toward the soma (Fig. 5, 1st stimulus *), whereas it was reported previously that the population spike propagated from the somatic region into apical and basal dendrites. The reason for this difference is not entirely clear, but possible factors to be considered include stimulus strength and location, temperature, and details of slice preparation. In particular, the angle at which slices were cut could influence local circuitry activated by the stimulus, such as feedforward inhibition that impinges on the soma and can thus impact the ability to generate a somatic spike (Pouille and Scanziani, 2001).

In addition to the convenience that multisite recordings offer for deriving CSD profiles from single responses, this multisite approach enables the application of CSD analysis for individual events that either can not be repeated, such as irregularly occurring spontaneous bursts or interictal spikes, or for stimuli that lead to irreversible changes, such as LTP (Mitzdorf, 1985; Richardson et al., 1986; Wheeler and Novak, 1986). In this regard, the CSD that we present of theta bursts (Fig. 5) represents a unique application of the recording configuration. We speculate that the enhancement and prolongation of the dendritic sinks during the later stimuli in a burst (Fig. 5, #) represents the recruitment of NMDA receptors that are initially blocked at hyperpolarized potentials. It will be useful to combine CSD analysis with complementary recording modalities and pharmacological tests to confirm this interpretation (Mann et al., 2005; Blake et al., 2007). It will also be useful to couple CSD analysis with imaging techniques to provide additional framework to study functional network activity.

The physical properties of PDMS, such as its hydrophobicity, and the use of low volumes, allow the creation of multiple openings in the perfusion chamber to provide access for electrophysiological equipment. Electrodes can be inserted through these “virtual walls” without breaking the surface tension. Other benefits of using PDMS and the construction techniques described herein are versatility, durability, and low cost. By altering the thickness of layer 2, and modifying the size of the opening in this layer, the chamber can be made to accommodate a variety of brain slice geometries and thicknesses. The materials are

inexpensive (though specialized equipment for making new masks is necessary), and both the chambers and the recording electrodes can be re-used may times, further reducing costs.

Just as recording chamber technology continues to improve, so too does electrode technology – particularly for performing multisite recordings *in vivo*. The approach that we describe here should be easily adapted to take advantage of these advances. The use of multi-shank recording electrodes will permit two-dimensional, and even three-dimensional, CSD analysis (Wheeler and Novak, 1986; Buzsáki, 2004). The incorporation of "tetrodes" will make it possible to record single units as well as field potentials, to aid investigations of the genesis of network oscillations (Csicsvari et al., 2003B). Introduction of multisite stimulating electrodes with precisely timed and spaced inputs will facilitate studies of integrative function. This perfusion chamber design can also serve as an *in vitro* model for screening drugs acting on the network level (Weiss et al., 2003), and the delivery of pharmacological agents to restricted regions of the slice, as laminar flow chambers permit (Blake et al., 2007), should also aid in studies of the roles played by ion channels distributed along the somatodendritic axis in integrative neuronal function. It is likely that additional uses for microfluidics, multisite recordings, and brain slice recordings will emerge in the coming years. The chamber design that we report here can play a role in bringing together all of these advances.

Acknowledgments

The authors would like to thank Luke Bassuener for providing the drawing in Fig. 1C, and Mark Perkins for excellent technical assistance. This research was supported by National Institutes of Health grants P01-GM47818 and R01-NS56411 to R.A. Pearce and by National Institutes of Health grants KL2-RR025012 and R21-NS051580 to J.C. Williams.

AJB, TMP, TRP, and JCW designed and fabricated the perfusion chambers; FCR, AB, EDZ, and RAP performed electrophysiological experiments; FCR, JAH, and AJB analyzed electrophysiological data; and AJB, FCR, EDZ, RAP, and JCW wrote the manuscript.

References

Aitken PG, Breese GR, Dudek FF, Edwards F, Espanol MT, Larkman PM, Lipton P, Newman GC, Nowak TS, Panizzon KL Jr. Raley-Susrnan KL, Reid KH, Rice ME, Sarvey JM, Schoepp DD, Segal M, Taylor CP, Teyler TJ, Voulalas PJ. Preparative methods for brain slices: a discussion. J. Neuro. Methods. 1995; 59:139–49.

Beebe DJ, Moore JS, Yu Q, Liu RH, Kraft ML, Jo BH, Devadoss C. Microfluidic tectonics: A comprehensive construction platform for microfluidic systems. Proc. Natl. Acad. Sci. USA. 2000; 97:13488–93. [PubMed: 11087831]

Beebe DJ, Mensing GA, Walker GM. Physics and applications of microfluidics in biology. Annu. Rev. Biomed. Eng. 2002; 4:261–86. [PubMed: 12117759]

Berdichevsky Y, Sabolek H, Levine JB, Staley KJ, Yarmush ML. Microfluidics and multielectrode array-compatible organotypic slice culture method. J. Neurosci. Methods. 2009; 178:59–64. [PubMed: 19100768]

Bjornsson CS, Oh SJ, Al-Kofahi YA, Lim YJ, Smith KL, Turner JN, De S, Roysam B, Shain W, Kim SJ. Effects of insertion conditions on tissue strain and vascular damage during neuroprosthetic device insertion. J. Neural Eng. 2006; 3:196–207. [PubMed: 16921203]

Blake AJ, Pearce TM, Rao NS, Johnson SM, Williams JC. Multilayer PDMS microfluidic chamber for controlling brain slice microenvironment. Lab on a Chip. 2007; 4:842–849. [PubMed: 17594002]

Boppart SA, Wheeler BC, Wallace CS. A flexible perforated microelectrode array for extended neural recordings. IEEE Trans. Biomed. Eng. 1992; 39:37–42. [PubMed: 1572679]

Bragin A, Hetke J, Wilson CL, Anderson DJ, Engel J Jr. Buzsáki G. Multiple site silicon-based probes for chronic recordings in freely moving rats: implantation, recording and histological verification. J. Neurosci. Methods. 2000; 98:77–82. [PubMed: 10837874]

Buzsáki G, Czopf J, Kondákor I, Kellényi L. Laminar distribution of hippocampal rhythmic slow activity (RSA) in the behaving rat: current-source density analysis, effects of urethane and atropine. Brain Res. 1986; 365:125–37. [PubMed: 3947979]

Buzsáki G. Large-scale recording of neuronal ensembles. Nature Neuro. 2004; 7:446–51.

Csicsvari J, Jamieson B, Wise KD, Buzsáki G. Mechanisms of gamma oscillations in the hippocampus of the behaving rat. Neuron. 2003A; 37:311–22. [PubMed: 12546825]

Csicsvari J, Henze DA, Jamieson B, Harris KD, Sirota A, Bartho P, Wise KD, Buzsáki G. Massively Parallel Recording of Unit and Local Field Potentials With Silicon-Based Electrodes. J. Neurophysiol. 2003B; 90:1314–23. [PubMed: 12904510]

Drake KL, Wise KD, Farraye J, Anderson DJ, Bement SL. Performance of planar multisite microprobes in recording extracellular single-unit intracortical activity. IEEE Trans. Biomed. Eng. 1988; 35:719–32. [PubMed: 3169824]

Duffy DC, McDonald JC, Schueller O, Whitesides GM. Rapid prototyping of microfluidic systems in poly(dimethylsiloxane). Anal. Chem. 1998; 70:4974–84. [PubMed: 21644679]

Freeman JA, Nicholson C. Experimental optimization of current source-density technique for anuran cerebellum. J. Neurophysiol. 1975; 38:369–82. [PubMed: 165272]

Gholmieh G, Soussou W, Han M, Ahuja A, Hsiao M, Song D, Tanguay AR Jr. Berger TW. Custom-designed high-density conformal planar multielectrode arrays for brain slice electrophysiology. J. Neurosci. Methods. 2006; 152:116–29. [PubMed: 16289315]

Hájos N, Pálhalmi J, Mann EO, Németh B, Paulsen O, Freund TF. Spike Timing of distinct types of GABAergic interneuron during hippocampal gamma oscillations in vitro. J. Neurosci. 2004; 24:9127–37. [PubMed: 15483131]

Hájos N, Ellender TJ, Zemankovics R, Mann EO, Exley R. Maintaining network activity in submerged hippocampal slices: importance of oxygen supply. Eur. J. Neurosci. 2009; 29:319–27. [PubMed: 19200237]

Heuschkel MO, Fejtl M, Raggenbass M, Bertrand D, Renaud P. A three-dimensional multi-electrode array for multi-site stimulation and recording in acute brain slices. J. Neurosci. Methods. 2002; 114:135–48. [PubMed: 11856564]

Huchzermeyer C, Albus K, Gabriel H, Otáhal O, Taubenberger N, Heinemann U, Kovács R, Kann O. Gamma oscillations and spontaneous network activity in the hippocampus are highly sensitive to decreases in pO_2 and concomitant changes in mitochondrial redox state. J. Neurosci. 2008; 28:1153–62. [PubMed: 18234893]

Jo B, Van Lerberghe LM, Motsegood KM, Beebe DJ. Three-dimensional micro-channel fabrication in polydimethylsiloxane (PDMS) elastomer. J. MEMS. 2000; 9:76–81.

Larson J, Wong D, Lynch G. Patterned stimulation at the theta frequency is optimal for the induction of hippocampal long-term potentiation. Brain Res. 1986; 368:347–50. [PubMed: 3697730]

Lipton P, Aitken PG, Dudek FE, Eskessen K, Espanol MT, Ferchmin PA, Kelly JB, Kreisman NR, Landfield PW, Larkman PM. Making the best of brain slices: comparing preparative methods. J. Neurosci. Methods. 1995; 59:151–6. [PubMed: 7475245]

Mann EO, Suckling JM, Hájos N, Greenfield SA. Perisomatic feedback inhibition underlies cholinergically induced fast network oscillations in the rat hippocampus in vitro. Neuron. 2005; 45:105–17. [PubMed: 15629706]

Mitzdorf U. Current source-density method and application in cat cerebral cortex: investigation of evoked potentials and EEG phenomena. Physiol. Rev. 1985; 65:37–100. [PubMed: 3880898]

Mohammed JS, Caicedo HH, Falla CP, Eddington DT. Microfluidic add-on for standard electrophysiology chambers. Lab on a Chip. 2008; 8:1048–55. [PubMed: 18584078]

Nam Y, Wheeler BC, Heuschkel MO. Neural recording and stimulation of dissociated hippocampal cultures using microfabricated three-dimensional tip electrode array. J. Neurosci. Methods. 2006; 178:296–99. [PubMed: 16494949]

Passeraub PA, Almeida AC, Thakor NV. Design, micro-fabrication and analysis of a microfluidic chamber for the perfusion of brain tissue slices. Biomed. Microdev. 2003; 5:147–55.

Pearce RA. Physiological evidence for two distinct GABA responses in rat hippocampus. Neuron. 1993; 10:189–200. [PubMed: 8382497]

Pearce RA. Volatile anaesthetic enhancement of paired-pulse depression investigated in the rat hippocampus in vitro. J. Phys. 1996; 492:823–40.

Pettersen KH, Devor A, Ulbert I, Dale AM, Einevoll GT. Current-source density estimation based on inversion of electrostatic forward solution: effects of finite extent of neuronal activity and conductivity discontinuities. J. Neurosci. Methods. 2006; 154:116–33. [PubMed: 16436298]

Pouille F, Scanziani M. Enforcement of temporal fidelity in pyramidal cells by somatic feed-forward inhibition. Science. 2001; 293:1159–63. [PubMed: 11498596]

Rambani K, Vukasinovic J, Glezer A, Potter SM. Culturing thick brain slices: An interstitial 3D microperfusion system for enhanced viability. J. Neurosci. Methods. 2009; 180:243–54. [PubMed: 19443039]

Richardson TL, Turner RW, Miller JJ. Action-potential discharge in hippocampal CA1 pyramidal neurons: current source-density analysis. J. Neurophys. 1987; 58:981–96.

Rutten W, Mouveroux J, Buitenweg J, Heida C, Ruardij T, Marani E, Lakke E. Neuroelectronic interfacing with cultured multielectrode arrays toward a cultured probe. Proc. IEEE. 2001; 89:1013–29.

Sarvey JM, Burgard EC, Decker G. Long-term potentiation: studies in the hippocampal slice. J. Neurosci. Methods. 1989; 28:109–24. [PubMed: 2542698]

Sniadecki NJ, Chen CS. Microfabricated silicone elastomeric post arrays for measuring traction forces of adherent cells. Methods in Cell Biology. 2007; 83:313–328. [PubMed: 17613314]

Steidl EM, Neveu E, Bertrand D, Buisson B. The adult rat hippocampal slice revisited with multi-electrode arrays. Brain Res. 2006; 1096:70–84. [PubMed: 16716268]

Taube JS, Schwartzkroin PA. Mechanisms of long-term potentiation: a current-source density analysis. J. Neurosci. 1988; 8:1645–55. [PubMed: 3367214]

Traub RD, Miles R, Wong RK. Model of the origin of rhythmic population oscillations in the hippocampal slice. Science. 1989; 243:1319–25. [PubMed: 2646715]

Vetter RJ, Williams JC, Hetke JF, Nunamaker EA, Kipke DR. Chronic neural recording using silicon-substrate microelectrode arrays implanted in cerebral cortex. IEEE Trans. Biomed. Eng. 2004; 51:896–904. [PubMed: 15188856]

Vida I, Czopf J, Czéh G. A current-source density analysis of the long-term potentiation in the hippocampus. Brain Res. 1995; 671:1–11. [PubMed: 7728519]

Weiss T, Veh RW, Heinemann U. Dopamine depresses cholinergic oscillatory network activity in rat hippocampus. Eur. J. Neurosci. 2003; 18:2573–80. [PubMed: 14622158]

Ward MP, Rajdev P, Ellison C, Irazoqui PP. Toward a comparison of microelectrodes for acute and chronic recordings. Brain Res. 2009:1–19. In Press.

Wheeler BC, Novak JL. Current source density estimation using microelectrode array data from the hippocampal slice preparation. IEEE Trans. Biomed. Eng. 1986; 33:1204–12. [PubMed: 3817854]

Wu C, Luk WP, Gillis J, Skinner F, Zhang L. Size does matter: generation of intrinsic network rhythms in thick mouse hippocampal slices. J. Neurophysiol. 2005; 93:2302–17. [PubMed: 15537814]

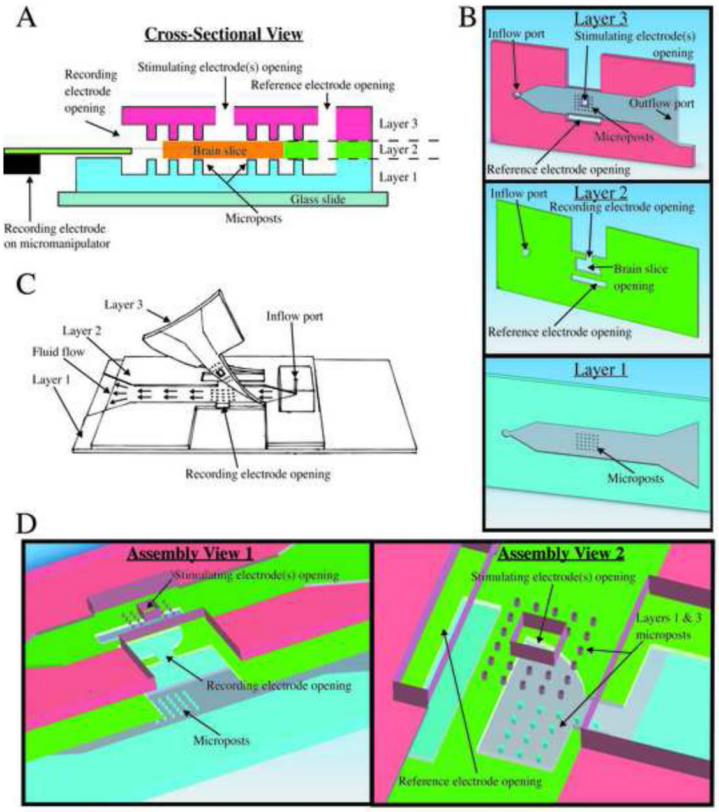

Fig. 1.

Microfluidic perfusion chamber design. (A) A cross-section at the center of the microposts reveals the locations of the electrode openings relative to the brain slice and the different layer features. (B) A computer aided design (CAD) model displays the distinct features from a bottom surface view for each individual layer. (C) A free-hand drawing shows how the device appears after each layer is assembled and how the top layer is partially bonded only at the front. This allows a brain slice to be positioned properly at the electrode openings before the PDMS is temporarily sealed for perfusion to commence. (D) A CAD model shows an exploded three-dimensional view of layers and provides an idea of how alignment of the top and side openings is necessary for the integrity of the chamber.

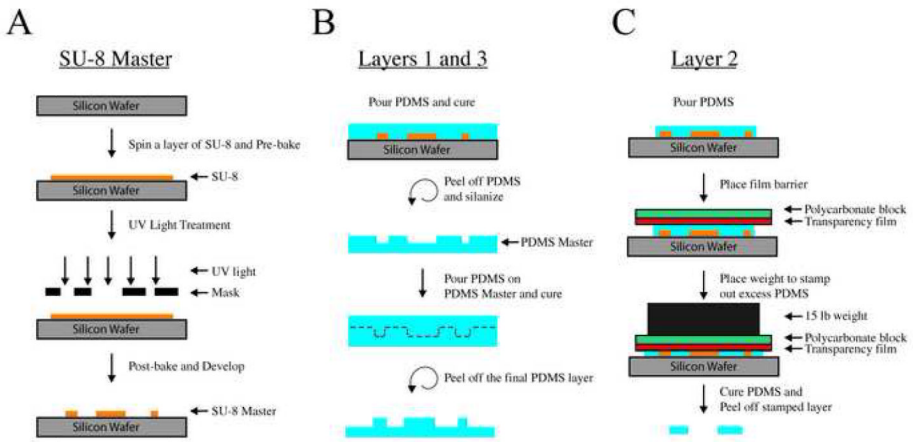

Fig. 2.

Microfluidic perfusion chamber fabrication process. (A) A unique SU-8 master is constructed for each layer, layer 2 is depicted. The SU-8 is spun onto a silicon wafer at a set speed that correlates with a desired thickness. After spinning the SU-8, a mask design, distinct for each layer, is used in conjunction with a UV light to project the mask design onto the SU-8, where exposed SU-8 crosslinked. Each layer has a different SU-8 master that is used to make a PDMS mold for each layer. (B) Layers 1 and 3 use a double-negative PDMS molding process, as shown here for layer 1. This process involves creating a PDMS master from the SU-8 master that enables the reliable production of microposts since the PDMS master is more flexible. (C) A “cookie-cutter” method is used to cut out the PDMS for layer 2. (D) Layer 1 uses a single mask, whereas layer 3 uses two masks that define the electrode openings.

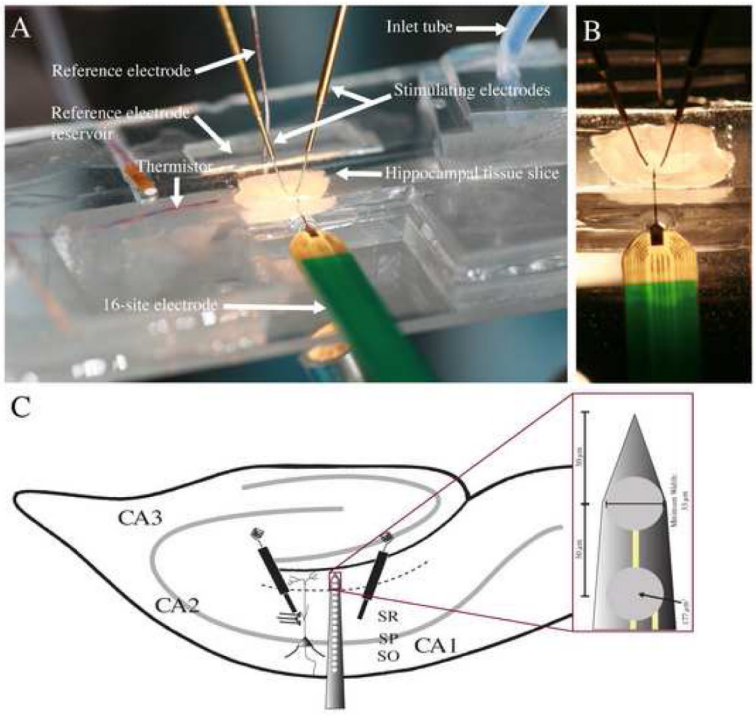

Fig. 3.

Experimental Setup. (A) Photograph of the experimental setup, showing the arrangement of electrodes used to stimulate and record from a hippocampal brain slice. (B) Higher magnification photograph. The recording electrode is inserted through the side opening into the edge of the hippocampal slice; stimulating electrodes are inserted through the top opening. (C) A schematic diagram of the hippocampus with a 16-channel recording electrode and two stimulating electrodes in place. The recording probe is inserted perpendicularly to the hippocampal layers, allowing for simultaneous data collection along the somatodendritic axis of pyramidal neurons. Stimulating electrodes are placed in *stratum radiatum* to stimulate axons of the Schaffer collateral pathway. Inset; Expanded view of the tip of the NeuroNexus probe that describes recording site characteristics. SO: *stratum oriens*; SP: *stratum pyramidale*; SR: *stratum radiatum*.

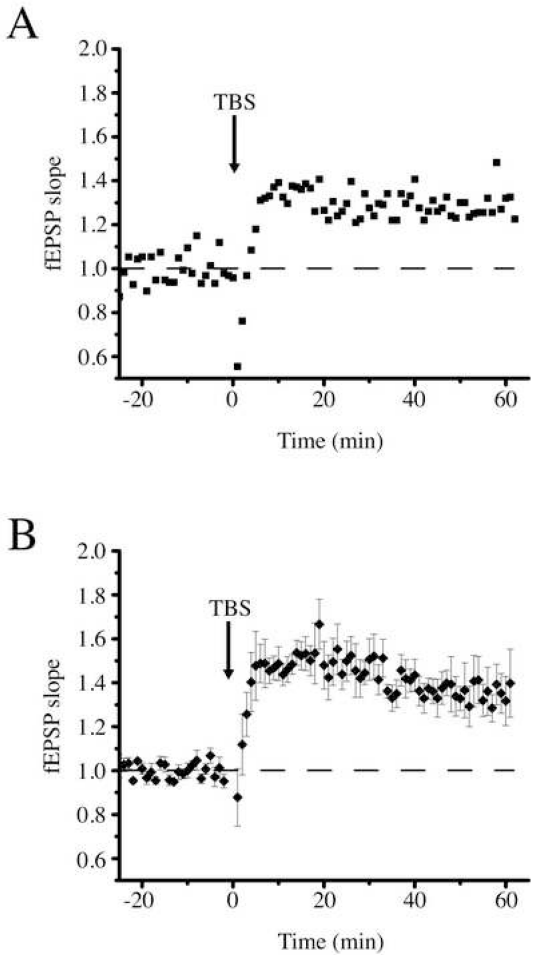

Fig. 4.

Measurement of long-term potentiation using a 16-channel recording electrode. (A) Single field excitatory potentials (fEPSPs) at each of the 16 recording sites before (left) and after (right) theta burst stimulation (TBS). The channel with the greatest rising slope (thick line) was used for fEPSP slope measurements. Scale bar: 1 mV, 20 ms. Approximate locations of recording sites are designated by letter code: HF hippocampal fissure; SLM *stratum lacunosum-moleculare*; SR *stratum radiatum*; *SP stratum pyramidale*; SO *stratum oriens*; ALV alveus. (B) Effect of TBS on fEPSP slope in the experiment illustrated in panel A. Responses were normalized to the mean response during the 20-minute baseline period. (C) Average effect of TBS on fEPSP slope in four different experiments. Error bars represent standard deviation.

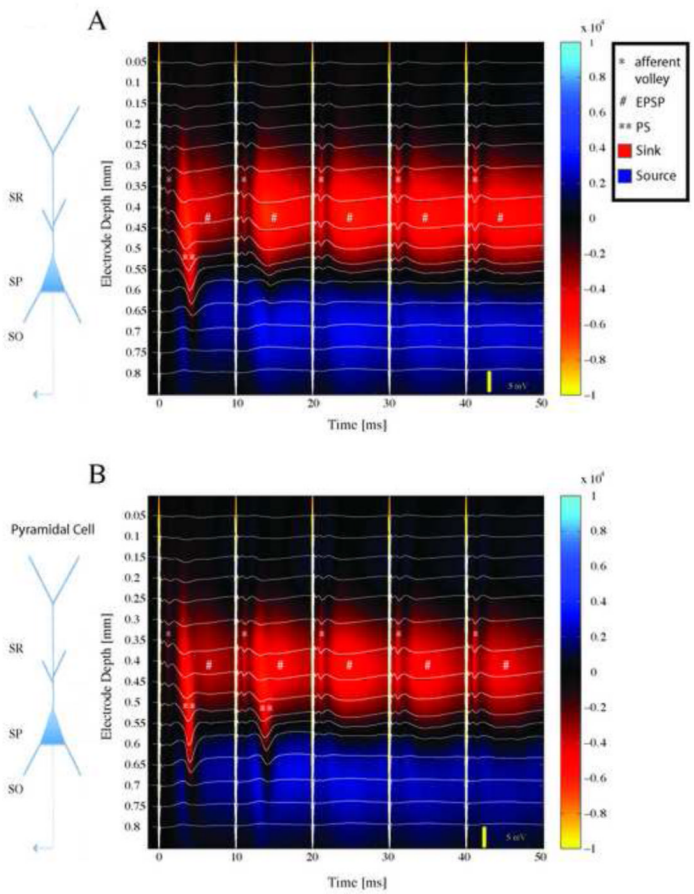

Fig. 5.

Laminar profiles of the field potentials evoked during theta-burst stimulation, and the corresponding current source density (CSD) analysis. Evoked potentials (white traces) are superimposed on pseudo-color images of CSD profiles. Warm colors represent current sinks, cool colors current sources. Thick vertical white lines are stimulus artifacts. A schematic diagram of a pyramidal cell is shown to the left, with corresponding hippocampal layers labeled SR-*stratum radiatum*, SP-*stratum pyramidale*, SO-*stratum oriens*. (A) Response to the first burst of the first train. The first stimulus in the burst elicited a brief sink in SR corresponding to the fiber volley (*), followed by a field excitatory postsynaptic potential (fEPSP) that propagated to the somatic region and resulted in a population spike (**). Subsequent stimuli elicited only fEPSPs (#). (B) The first burst of the third train. Responses are similar to the first burst (panel A) except that a current sink that propagated from the dendrites to the soma was evident following both the first and second stimuli in the burst.